Published on 09 June 2017. Downloaded by East China University of Science & Technology on 10/23/2020 8:47:44 AM.

Soft Matter

PAPER

View Article Online
View Journal | View Issue

Check for updates

Cite this: *Soft Matter*, 2017, **13**, 5130

Aqueous self-assembly of hydrophobic macromolecules with adjustable rigidity of the backbone†

Zhou Guan,‡[a] Dapeng Liu,‡[a] Jiaping Lin*[a] and Xiaosong Wang *[b]

Received 3rd June 2017,
Accepted 9th June 2017

DOI: 10.1039/c7sm01101f

rsc.li/soft-matter-journal

P(FpC_3P) (Fp: CpFe(CO)$_2$; C_3P: propyl diphenyl phosphine) has a helical backbone, resulting from piano stool metal coordination geometry, which is rigid with intramolecular aromatic interaction of the phenyl groups. The macromolecule is hydrophobic, but the polarized CO groups can interact with water for aqueous self-assembly. The stiffness of P(FpC_3P), which is adjustable by temperature, is an important factor influencing the morphologies of kinetically trapped assemblies. P(FpC_3P)$_7$ self-assembles in DMSO/water (10/90 by volume) into lamellae at 25 °C, vesicles at 40 °C and irregular aggregates at higher temperatures (60 and 70 °C). The colloidal stability decreases in the order of lamellae, vesicles and irregular aggregates. Dissipative particle dynamics (DPD) simulation reveals the same temperature-dependent self-assembled morphologies with an interior of hydrophobic aromatic groups covered with the metal coordination units. The rigid backbone at 25 °C accounts for the formation of the layered morphology, while the reduced rigidity of the same P(FpC_3P)$_7$ at 40 °C curves up the lamellae into vesicles. At a higher temperature (60 or 70 °C), P(FpC_3P)$_7$ behaves as a random coil without obvious amphiphilic segregation, resulting in irregular aggregates. The stiffness is, therefore, a crucial factor for the aqueous assembly of macromolecules without obvious amphiphilic segregation, which is reminiscent of the solution behavior observed for many hydrophobic biological macromolecules such as proteins.

Introduction

Supramolecular chemistry has been substantially developed with inspiration from nature.[1–4] Amphiphilic lipids have promoted substantial development in the synthesis and self-assembly of surfactants and block copolymers.[5–8] Many biological macromolecules, like DNA, RNA, and proteins, are hydrophobic without obvious amphiphilic features, which also assemble into various defined structures laced with a few groups interacting with water at the surface.[9–15] This assembly is strongly influenced by factors other than amphiphilic segregation, such as conformational flexibility.[16,17]

Many synthetic polymers are rigid, such as helical polypeptides, aromatic polyesters and conjugated polymers.[18–20] It is well known that rigid-coil block copolymers exhibit assembling behaviour substantially different from that of coil–coil amphiphilic block copolymers in terms of assembled nanostructures.[21–24] However, it is not easy to elucidate the effect of chain stiffness on the assembling process, because the segregation of the amphiphilic blocks is usually overwhelming. Macromolecular building blocks with adjustable rigidity and no obvious amphiphilic segments, reminiscent of some biological species, will be an ideal system to investigate the effect of stiffness on self-assembly, but this type of macromolecule is rarely available.

P(FpC_3P) (Fp: CpFe(CO)$_2$; C_3P: propyl diphenyl phosphine) is a macromolecule synthesized by migration insertion polymerization (MIP) of FpC_3P (Scheme 1). As illustrated in Scheme 1, the backbone of P(FpC_3P) is constructed from the connection of phosphine coordinated Fp acyl repeating units that have a piano stool coordination geometry.[25–27] The polymer adopts a helical conformation,[27] and the phenyl groups from

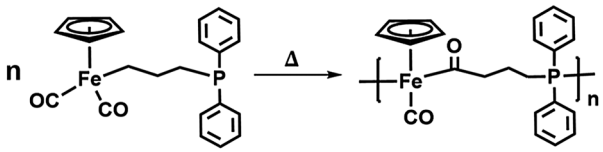

Scheme 1 Synthesis of P(FpC_3P)$_n$ by migration insertion polymerization.

[a] Shanghai Key Laboratory of Advanced Polymeric Materials, State Key Laboratory of Bioreactor Engineering, Key Laboratory for Ultrafine Materials of Ministry of Education, School of Materials Science and Engineering, East China University of Science and Technology, Shanghai, 200237, China. E-mail: jlin@ecust.edu.cn
[b] Department of Chemistry and Waterloo Institute for Nanotechnology (WIN), University of Waterloo, 200 University Ave, Waterloo, ON, N2L 3G1, Canada. E-mail: xiaosong.wang@uwaterloo.ca

† Electronic supplementary information (ESI) available. See DOI: 10.1039/c7sm01101f

‡ These authors contributed equally to this work.

This journal is © The Royal Society of Chemistry 2017

Published on 09 June 2017. Downloaded by East China University of Science & Technology on 10/23/2020 8:47:44 AM.

the neighbouring repeating units closely interact with each other.[27] The strength of this aromatic interaction can be varied by solvation conditions,[27] which may be a variable adjusting the stiffness of P(FpC_3P).

P(FpC_3P), regardless of the degree of polymerization (DP), is soluble in THF.[28] When water is added to a THF solution, P(FpC_3P) assembles into vesicles with the CO groups interacting with water.[28] DMSO, however, is a marginal solvent. P$(FpC_3P)_{64}$ with a DP of 64 is soluble in DMSO only at an elevated temperature.[26] Temperature is, therefore, a parameter adjusting the solvent–polymer interaction, which will, in turn, affect the stiffness of the macromolecules. The degree of solvation of P$(FpC_3P)_7$ with a DP of 7 can be adjusted in the temperature range from 25 °C to 70 °C,[26] so it is expected that the effect of temperature on the chain stiffness and assembling behaviour can be studied. Theoretical simulations are necessary to assist the investigation,[29,30] because the theory underlying the aqueous self-assembly of homopolymers without water-soluble groups is undeveloped.[31–34] To investigate the effect of chain stiffness, the temperature-dependent chain conformation is quantitatively correlated with the stiffness of the backbone using both all-atom and dissipative particle dynamics (DPD) simulations.[35–38]

Herein, we report that P$(FpC_3P)_7$ can be varied from a rigid backbone at 25 °C to a less rigid chain at 50 °C and a random coil at 70 °C. The effect of this temperature-dependent rigidity on the assembly of P$(FpC_3P)_7$ in DMSO/water (10/90 by volume) is discovered. Regardless of the temperature, the molecules associate into a sandwich structure with an interior of the aromatic groups covered with the metal coordination groups. The rigidity of the backbone at 25 °C directs the sandwich structures into lamellae. By increasing the temperature to 40 °C, the reduced rigidity of the chain allows the membranes to curve up forming vesicles. At a higher temperature (60 or 70 °C), P$(FpC_3P)_7$ is a random coil without obvious amphiphilic segregation and the sandwich aggregates appear to be irregular particles.

Results and discussion

Temperature-dependent chain conformation of P$(FpC_3P)_7$

To reveal the chain conformation in response to temperature, all-atom simulations were performed using Materials Studio.[27] Fig. 1 shows the conformation of P$(FpC_3P)_7$ in water at equilibrium states. As shown in Fig. 1a, an alpha-helical structure is observed at 25 °C and the average distance for the neighbouring aromatic groups is *ca.* 4.7 Å, indicating a strong p–p interaction. Upon increasing the temperature to 50 °C, the aromatic pendent groups do not interact in the same fashion and the distance between them increases to 5.9 Å (Fig. 1b), suggesting that the helical sense of the chain is weakened. The chain appears to be a random coil without any obvious alpha-helix at 70 °C (Fig. 1c) and the distance between the aromatic groups is 7.3 Å. This simulation reveals that both the aromatic interaction and chain conformation of P$(FpC_3P)_7$ are temperature-dependent.

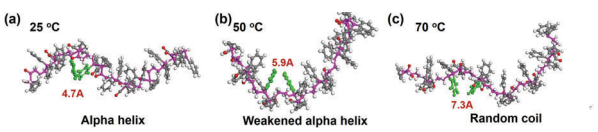

Fig. 1 Chain conformation of P$(FpC_3P)_7$ in response to temperature. The green groups represent two neighboring phenyl rings and the red numbers indicate the distances between the groups.

Temperature-dependent self-assembly of P$(FpC_3P)_7$

To evaluate the effect of temperature-dependent chain conformation on the self-assembly, solutions of P$(FpC_3P)_7$ (1 mg mL^{-1}) were prepared in DMSO/water (1/9 by volume) at various temperatures. The resultant assemblies were characterized by DLS, AFM and TEM. P$(FpC_3P)_7$ assembled at 25 °C into aggregates with apparent hydrodynamic diameters (D_h) of *ca.* 86 nm and a PDI of 0.21 (Fig. S1a, ESI†). The AFM image, as shown in Fig. 2a, indicates that the size of the P$(FpC_3P)_7$ assemblies is *ca.* 70 nm. The height profile (Fig. 2b and c) reveals that the thickness of the aggregates is *ca.* 3.5 nm. The ratio of size to thickness (23) is high and confirms nano-sheets obtained. The TEM images, as shown in Fig. 2d and Fig. S1b (ESI†), also display a layered structure, but the size is over a few micrometers (Fig. 2d). The larger size observed in the TEM images is attributed to the fusion of the nano-sheets (Fig. S1b, ESI†) resulting from the drying effect. The AFM samples were prepared by spin coating, which minimized the drying effect resulting in the measured size comparable with the D_h (Fig. S1a, ESI†). Although the assemblies were fairly stable, they started to precipitate three weeks later. It suggests that the nano-sheet is a kinetically trapped morphology.

P$(FpC_3P)_7$ assemblies prepared at 40 °C have a D_h of 98 nm with a PDI of 0.361 as indicated by DLS analysis (Fig. S2a, ESI†). No obvious change in the DLS profile was observed when the sample was cooled to room temperature in 15 minutes. However, a small fraction of large aggregates were formed in a few days and precipitates were observed in 2 weeks. The assemblies were, therefore, less stable as compared to those assembled at 25 °C. Right after cooling, a TEM sample was prepared and examined (Fig. 3 and Fig. S2b–d, ESI†). As shown in Fig. 3a and b, some spherical aggregates with a contrast between the periphery and the centre are observed, suggesting that nano-vesicles are formed. The thickness of the wall is *ca.* 3.2 nm, which is similar to the height of the nano-sheet obtained at 25 °C. Interestingly, many collapsed nano-vesicles with severe indentations and distortions also appear in the TEM images (Fig. 3a and Fig. S2, ESI†).

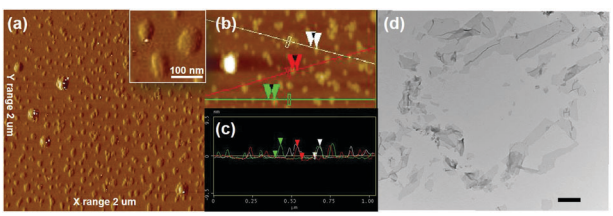

Fig. 2 (a) AFM phase mode image, (b) height mode image, (c) height profile along the line in (b) (the full scale of the *Y* axis is 9.5 nm) and (d) TEM image for P$(FpC_3P)_7$ nanosheets assembled at 25 °C in DMSO/H_2O (10/90 by volume) solution (0.1 mg mL^{-1}). Scale bar for TEM: 500 nm.

Published on 09 June 2017. Downloaded by East China University of Science & Technology on 10/23/2020 8:47:44 AM.

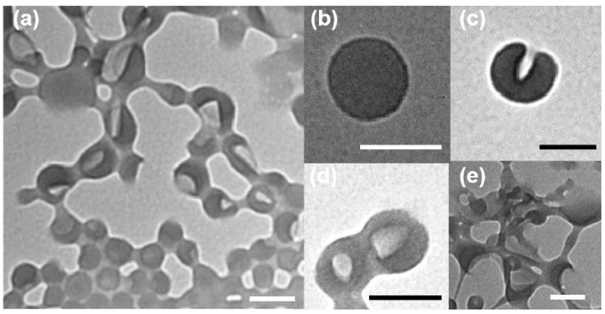

Fig. 3 (a–e) TEM images of $P(FpC_3P)_7$ nano-vesicles assembled at 40 °C in DMSO/H_2O (10/90 by volume) solution (0.1 mg mL^{-1}). Scale bar: 100 nm.

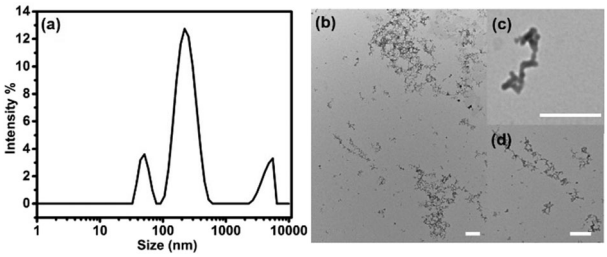

Fig. 4 (a) The DLS profile and (b–d) TEM images of $P(FpC_3P)_7$ aggregates assembled at 70 °C in DMSO/H_2O (10/90 by volume) solution (0.1 mg mL^{-1}). Scale bar: 100 nm.

Fig. 3c and d show that the vesicle has a bowl-shape. The side view indicates that the periphery is relatively dark (Fig. 3c), suggesting that the wall of the vesicles is not broken. Block copolymer bowl-shaped vesicles were reported before, which was formed during the sample preparation for TEM experiments.[39] When the sample was dried in a high vacuum, the pressure gradient between the two sides of the vesicles caused the deformation of the vesicles. The bowl-shaped vesicles can also be formed during the addition of water to a solution of block copolymers in a common solvent.[40–42] The diffusion of the common solvent through the vesicular wall induces a negative pressure within the cavity, which causes the deflation of spherical vesicles. The evaporation of DMSO/water under ambient conditions is slow and may not be able to generate a pressure deforming the vesicle. The bowl-shaped vesicles are, therefore, formed during the addition of water to the DMSO solution. In addition to the deformed vesicles, we also captured some vesicles with ruptured walls as shown in the TEM images (Fig. 3e and Fig. S2c, ESI†).

$P(FpC_3P)_7$ assemblies prepared at 60 °C have a D_h of *ca.* 71 nm with a PDI of 0.236 (Fig. S3, ESI†). TEM images indicated that irregular aggregates were formed (Fig. S4a, ESI†). We also noticed that the irregular aggregates, unlike the aggregates formed at other temperatures, were not stable and easily broken when exposed to the electron beam (Fig. S4b–d, ESI†). Further increasing the assembling temperature to 70 °C, the molecule assembled into aggregates with three size populations from 50 nm to 4500 nm as indicated in the DLS profile (Fig. 4a). As shown in the TEM image (Fig. 4b), the aggregates appear to be worm-like structures (Fig. 4c). Many of them are connected together (Fig. 4d), which may exist in the solution as large aggregates are detected by DLS analysis (Fig. 4a). The samples prepared at 60 and 70 °C precipitate in a week because of the hydrophobicity of the macromolecules. It is worth noting that the colloidal stabilities of the assemblies prepared at 25 and 40 °C are relatively higher. This difference can be attributed to the varied degree of hydrophobic hydration, which depends on the assembled structure.

Self-assembled morphologies reproduced by simulation

To simulate the self-assembling behaviour, DPD simulations were performed using a coarse-grained molecular model of $P(FpC_3P)_7$. As shown in Fig. 5a, COFeCO and $(CH_2)_3P$ are grouped as polar beads of O (yellow) and P (red), respectively, while the phenyl and Cp are denoted as hydrophobic beads of R (green). Fig. 5b displays the coarse-grained chain, which shows a metal coordination backbone with the hydrophobic beads as side groups. The repulsive parameter (a_{ij}) of the hydrophobic beads (R groups) with the backbone (O and P groups) and solvents is denoted as a_{RO}, a_{RP}, and a_{RS}, respectively, which is calculated from the Flory–Huggins parameter (χ_{ij}) and listed in Table S1 (ESI†).[43] The value for χ_{ij} in response to temperature is calculated using Materials Studio v8.0.27.

The all-atom simulations have suggested that the backbone is helical and rigid. In the DPD simulation, we regulated this rigidity by the strength of a three-body angle potential (denoted by k_c) to the backbone (formed by O and P groups). The larger the k_c, the stronger the chain stiffness. To confirm that the variation of k_c from 0 to $5k_BT$ can effectively capture the evolutionary rigidity of the chain in a DPD simulation, the persistence length (l_p) of a single chain, proportional to the stiffness,[37] is calculated using both all-atom and DPD simulations. The l_p in response to temperature varying from 25 to 70 °C (calculated from the all-atom simulation) and the profile of l_p as a function of k_c (calculated from the DPD simulation) are compared in Fig. 6. As shown in Fig. 6, the profiles (l_p vs k_c and l_p vs temperature) calculated from the two simulations are similar. The l_p is larger at 25 °C (all atom simulation) and a k_c of $5k_BT$ (DPD simulation), which gradually decreases with increase in temperature or decrease in k_c. At 60 °C or a k_c of 0, the l_p decreases to the minimum value and leaves off. The chain conformations in response to the k_c simulated from the DPD simulation of a single chain are also similar to those simulated from all-atom simulation (Fig. 6). The similarity of these two calculations elaborates that the temperature-dependent chain

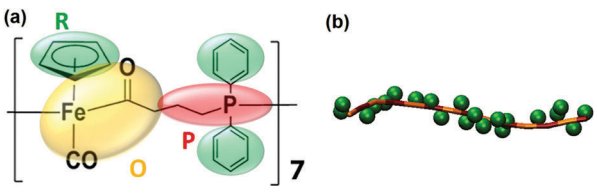

Fig. 5 Schematic illustration for the coarse-grained model of $P(FpC_3P)_7$ used for DPD simulation. (a) Coarse-grained groups for $P(FpC_3P)_7$ (green, orange and red beads represent benzyl/Cp, COFeCO, and $(CH_2)_3P$ groups, respectively). (b) Coarse-grained $P(FpC_3P)_7$ chain.

This journal is © The Royal Society of Chemistry 2017

Published on 09 June 2017. Downloaded by East China University of Science & Technology on 10/23/2020 8:47:44 AM.

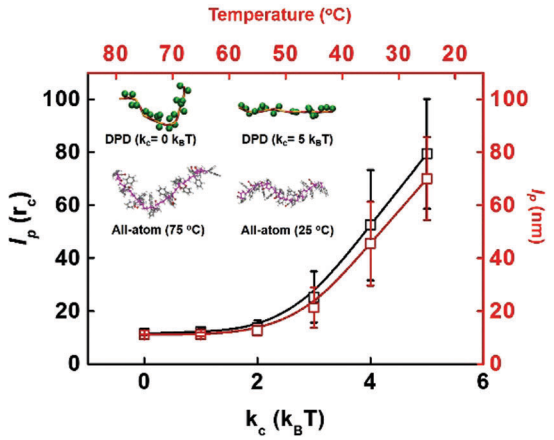

Fig. 6 Persistence length as a function of k_c in DPD simulation (the black curve) and temperature in all-atom simulation (the red curve). The chain conformations at 25 and 70 °C, corresponding to the k_c values of $5k_BT$ and $0k_BT$, are shown in the figure.

conformation is caused by the variation in the rigidity of the backbone, which is a parameter crucial for the assembly of $P(FpC_3P)_7$.

DPD simulation of the assembly in response to temperature was performed. Fig. 7a shows a lamella at the end of the simulation at 25 °C. The backbones of $P(FpC_3P)_7$ are aligned almost parallel to each other. As shown in the cross section of the lamella (Fig. 7b), the hydrophobic R groups (green) aggregate into a layer with the surfaces decorated with the polar O (orange) and P (red) groups. By examining the densities of these three groups along the normal direction (denoted by $x1$ in Fig. 7b), the R groups have one wider peak between the peaks for O and P groups, supporting a sandwich layered structure. As the thickness of the assembled nano-sheet is 3.2 nm as measured by AFM, it is likely that the sandwich membrane is a face-to-face assembly of two $P(FpC_3P)_7$ molecules. Fig. 7c shows the calculated order parameter (S) for $P(FpC_3P)_7$ backbone packing along the lamellae (denoted by $x2$). As shown in Fig. 7c, a relatively larger value of S (0.8, $0 \leq S \leq 1$) is observed, suggesting that the packing of $P(FpC_3P)_7$ backbones is highly ordered. The value of S (*ca.* 0.5) is slightly smaller, corresponding to a less ordered alignment, near the edges of the lamella (Fig. 7c). This reduced alignment is caused by the coverage of the polar group (O, P) on the high-energy edges to minimize the

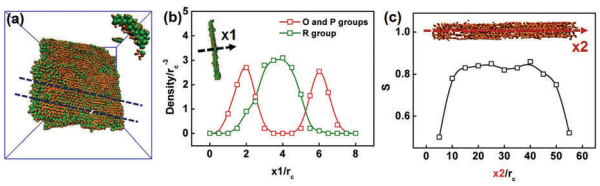

Fig. 7 (a) The simulated lamellar structure assembled at 25 °C ($k_c = 5k_BT$ and $a_{RO} = a_{RP} = 60$, $a_{RS} = 75$). The dashed lines indicate where the structure is sliced and enlarged for further analysis. (b) The densities of O, P and R groups along the cross section ($x1$ direction). (c) The order parameter of the backbones along the membrane plane ($x2$ direction).

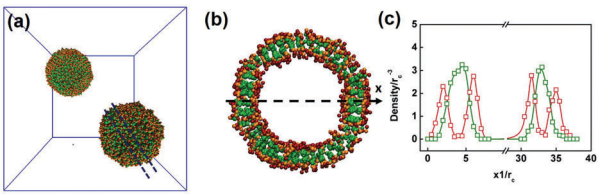

Fig. 8 (a) The simulated vesicular structure assembled at 40 °C ($k_c = 2k_BT$ and $a_{RO} = a_{RP} = 50$, $a_{RS} = 60$). The dashed lines indicate where the structure is sliced and enlarged for further analysis. (b) The cross section of the vesicle. (c) The densities of O, P and R groups along the cross section (x direction in (b)).

contact between the hydrophobic R groups and water. The formation of lamellar assemblies at 25 °C is, therefore, caused by the chain stiffness (Table S1, ESI†).

Fig. 8a and b display the morphology of $P(FpC_3P)_7$ assembled at 40 °C and the cross-sectional image. The density profiles for the polar O, P and hydrophobic R groups along the radial direction are displayed in Fig. 8c. As shown in the figures, the vesicular wall is also a sandwich structure similar to that for the lamellae formed at 25 °C, in which a hydrophobic domain of R groups (denoted by green) covered with the polar O (orange) and P (red) groups. The thickness of the vesicular wall as indicated in Fig. 8c is also similar to that for the lamella. The chain stiffness potential at 40 °C ($k_c = 2k_BT$) is lower than that at 25 °C ($k_c = 5k_BT$) (Table S1, ESI†), which allows the membrane to curve up forming vesicles to reduce the total free energy.

The assembling behaviour in response to the stiffness of $P(FpC_3P)_7$ was further investigated. We performed a simulation by adjusting the stiffness (k_c) of $P(FpC_3P)_7$ to $4k_BT$, a value between that at 25 °C ($5k_BT$) and that at 40 °C ($2k_BT$). As shown in Fig. 9a, the volumetric map image of the simulated assemblies indicates a curved lamella, which supports the observation that the reduced stiffness curves up the lamellae towards the vesicles (Fig. 9b). When the stiffness is adjusted to $1k_BT$, lower than that at 40 °C ($2k_BT$), the rigidity of the molecule is not sufficient to integrate the vesicular membrane, resulting in ruptured vesicles (Fig. 9c).

A higher temperature (either 60 or 70 °C) further reduces the bending energy of the macromolecular chain, so $P(FpC_3P)_7$ loses the rigidity (Table S1, ESI†) and takes a coil conformation (Fig. 1c). Consequently, the rigidity plays no role in the assembly at these two temperatures. As shown in Fig. 10a and b, the random coil aggregates into irregular particles. Both the experiment and

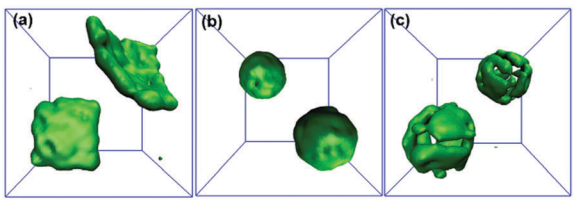

Fig. 9 Volumetric map images of (a) curved lamellae simulated with k_c of $4k_BT$, (b) vesicles simulated with k_c of $2k_BT$, and (c) ruptured vesicles simulated with k_c of $1k_BT$.

Published on 09 June 2017. Downloaded by East China University of Science & Technology on 10/23/2020 8:47:44 AM.

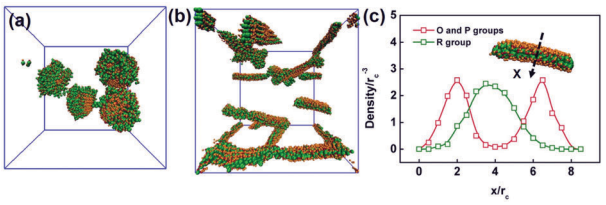

Fig. 10 (a) Simulated irregular aggregates assembled at 60 °C ($k_c = 0k_BT$ and $a_{RO} = a_{RP} = 40$, $a_{RS} = 50$), and (b) assembled at 70 °C ($k_c = 0k_BT$ and $a_{RO} = a_{RP} = 35$, $a_{RS} = 35$), and (c) densities of O, P and R groups along the x direction of one nanoparticle assembled at 70 °C.

simulation indicate that the aggregates formed at 70 °C (Fig. 4b and 10b) are larger than those formed at 60 °C (Fig. S4a, ESI,† and Fig. 10a), which is attributed to a lower de-solvation of the R groups and lower repulsive forces of R with O and P groups at 70 °C (Table S1, ESI†). The cross-section of the aggregates (Fig. 10c) also reveals a sandwich structure with the hydrophobic association of the R group. The packing density (Fig. 10c) is relatively lower as compared with that for the lamellae (Fig. 7b) due to the reduced segregation between the R groups with solvents, O and P groups. The sandwich structure suggests that the assembly is initiated by the hydrophobic association of the R groups. However, unlike amphiphilic molecules, the coil at a higher temperature lacks sufficient segregation forces to drive the assembly into defined nanostructures.

The DPD simulation has reproduced the self-assembled nanostructures at various temperatures, which helps us to elucidate the effect of the rigidity on the assembly (Fig. 11). $P(FpC_3P)_7$ assembles in the aqueous media into aggregates with hydrophobic aromatic groups aggregated and metal coordination polar backbones exposed to the solvents. As shown in Fig. 11, the stiffness of the chain at 25 °C directs the assembly into a layered structure. By decreasing the rigidity of the macromolecules at 40 °C, the layered structures start to curve and subsequently close-up forming vesicles. As the chain becomes flexible, the membrane of the vesicles is ruptured. At higher temperatures (60 and 70 °C), $P(FpC_3P)_7$ loses the rigidity and becomes a random coil without obvious amphiphilic segregation, the self-assembling is, therefore, only regulated by the hydrophobic interaction of the R groups, resulting in less ordered aggregates.

We have developed a reliable mapping method from a small-scaled molecular model (atomistic model) to a coarse-grained model for the macromolecule. For example, the chain stiffness was mapped *via* the persistence length, and the repulsive parameters in DPD simulations were mapped through the Flory–Huggins parameters. Like previous work,[29] this simulation approach effectively unveils the principles underlying the assembling behaviour of P(FpP).

Unlike the assembling behaviour of copolymers, it has rarely been reported that the same homopolymers assemble in aqueous media into different structures depending on the temperature-adjusted stiffness. However, it is not uncommon for natural materials. For example, the stiffness of DNA is important in protein–DNA binding specificity.[44] Some evidence also indicates that the persistence length of DNA is correlated with temperature.[45] Our discovery, therefore, provides guidance for the investigation of the environment-responsive behavior of natural macromolecules.

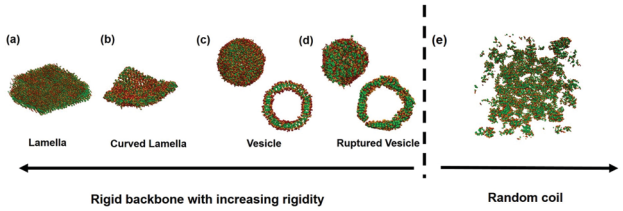

Fig. 11 The effect of stiffness on the morphologies self-assembled from hydrophobic macromolecules in aqueous media.

Conclusions

In summary, $P(FpC_3P)_7$ assembles in DMSO/water into kinetically trapped nano-sheets, vesicles and irregular aggregates at 25 °C, 40 °C and a higher temperature (60 or 70 °C), respectively. The irregular aggregates precipitated in a week, while the nano-sheets and vesicles are relatively stable. DPD simulation has reproduced this temperature-dependent assembling behaviour and indicates that the macromolecules pack into a sandwich structure with an interior of R groups covered with metal coordination polar groups. The rigidity of $P(FpC_3P)_7$ at 25 °C is a crucial parameter directing the assembly into a layered structure. The formation of the vesicles at 40 °C is due to the decrease in the rigidity. $P(FpC_3P)_7$ eventually loses the rigidity at a higher temperature (60 or 70 °C). Consequently, the hydrophobic molecules irregularly aggregate into precipitates. This experiment–simulation combined investigation establishes a basic theory for the effect of rigidity on the self-assembly of macromolecules without water-soluble groups, which will guide further research into the biomimetic supramolecular synthesis using hydrophobic macromolecules as building blocks.

Experimental

Materials and instrumentation

Sodium (Na), potassium (K), 1-bromo-3-chloropropane, and cyclopentadienyl iron dicarbonyl dimer (Fp2) were purchased from Sigma-Aldrich. Benzophenone was purchased from Fisher Scientific. DMSO was commercially available and used without further purification.

^1H, ^{31}P, and ^{13}C nuclear magnetic resonance (NMR) experiments were carried out on a Bruker-300 (300 MHz) spectrometer at an ambient temperature using either $CDCl_3$ or DMSO-d_6 as a solvent. NMR samples were prepared under a dry nitrogen atmosphere. Dynamic light scattering (DLS) measurements were carried out on a Malvern Zetasizer (Nano S90) with a laser wavelength of 633 nm. The auto measure mode was selected and the evaluation method was based on a standard Gaussian method. Transmission electron microscopy (TEM) experiments were performed using a transmission electron microscope (Philips CM10) with an acceleration voltage of 60 kV. TEM samples were

 This journal is © The Royal Society of Chemistry 2017

Published on 09 June 2017. Downloaded by East China University of Science & Technology on 10/23/2020 8:47:44 AM.

prepared by dipping a carbon-coated TEM copper grid into the solution of P(FpC3P) colloids, followed by drying in air. Atom force microscopy (AFM) experiments were performed using a Nanoscope MultiMode™ AFM microscope. The measurements were carried out in tapping mode using a conical AFM tip with a spring constant of 40 N m^{-1}, a resonance frequency of 300 kHz, and a tip radius of 8 nm. A freshly prepared colloidal solution was dropped onto a freshly cleaved mica substrate for spin-coating. The substrates were then dried at room temperature before the measurement.

Synthesis of $P(FpC_3P)_7$

$P(FpC_3P)_7$ was synthesized using a previously reported technique.[25–27] The polymerization of FpC_3P (*ca.* 1 g) was carried out in bulk at 70 °C for 20 h. The system was then cooled to room temperature. The crude product was first dissolved in a minimum amount of THF (*ca.* 5 mL) and then precipitated in a large amount of hexane (100 mL). The precipitates were collected *via* a filtration and dried under vacuum overnight at room temperature, yielding yellow powders. The resultant bright yellow powders were further characterized using NMR, IR and GPC. ^{1}H NMR (DMSO-d_6): 7.6–7.1 ppm (b, 10H, C_6H_5), 4.4–4.0 ppm (b, 5H, C_5H_5), 2.8–2.60 ppm (b, 1H, $COCH_2$), 2.4–2.1 ppm (b, 1H, $COCH_2$), 2.1–1.8 ppm (b, 2H, CH_2P), and 1.4–0.8 ppm (b, 2H, $CH_2CH_2CH_2$). ^{31}P NMR (DMSO-d_6): 73.2 ppm, 35.5 ppm. IR: 1910 cm^{-1} (terminal carbonyl groups), 1600 cm^{-1} (migrated carbonyl groups). GPC: M_n = 3320 g mol^{-1}; M_w = 3920 g mol^{-1}; PDI = 1.18.

Self-assembly of $P(FpC_3P)_7$

Self-assembly of $P(FpC_3P)_7$ was performed using DMSO as a co-solvent. A DMSO solution of $P(FpC_3P)_7$ (1 mg mL^{-1}) was prepared first. Then distilled water was added to the solution rapidly resulting in a colloidal solution. The final concentration of $P(FpC_3P)_7$ is 0.1 mg mL^{-1}. To investigate the effect of temperature on the assembly, the DMSO solution of $P(FpC_3P)_7$ and distilled water were first heated at a certain temperature for 24 h before they were used for the preparation of the colloids. We tried to remove DMSO by dialysis, but the colloids precipitated quickly during the dialysis due to their hydrophobicity.

All-atom simulation

The all-atom simulations were performed using molecular dynamics (MD). The simulation protocols were the same as used for our previous work.[27] One macromolecule was mixed with water molecules in a periodic simulation box. First, the system was optimized to minimize the free energy using the steepest descent method. Then molecular dynamics simulations were performed under an *NVT* ensemble in the temperature range from 25 to 75 °C. The Nosé thermostat was used to control the system temperature during the simulations. The COMPASS II force field was acted in the whole system, and the atom based summation method was applied to both van der Waals and Coulomb forces. The time step was set to be 1.0 fs and all the simulations were run for 10^4 ps. By mixing two different species in the simulation box and using the COMPASS II force field, the Flory–Huggins parameters (χ_{ij}) among different species were calculated.

DPD simulation system

DPD is a particle-based mesoscopic simulation technique for complex fluids.[43] In the simulation, each bead represents a block or cluster of atoms or molecules. The time evolution of the beads obeys Newton's equation of motion. In this equation, the total force is the sum of conservative, dissipative, and random forces. The simulations were conducted in a cubic box of 505 050 with periodic boundary conditions, and an *NVT* ensemble was adopted. Details regarding the simulations can be found in the ESI.†

Acknowledgements

The Natural Sciences and Engineering Research Council of Canada (NSERC RGPIN-2016-04497) and the University of Waterloo are acknowledged for financial support. This work was also supported by the National Natural Science Foundation of China (51303055, 21234002, and 21474029) and Shanghai Municipality (16520721900 and 14DZ2261205). D.-P. Liu is grateful for the financial support from the China Scholarship Council.

References

1 J.-M. Lehn, *Supramol. Chem.*, VCH, Weinheim, 1995, vol. 1.
2 J. M. Lehn, *Angew. Chem., Int. Ed. Engl.*, 1988, **27**, 89–112.
3 I. V. Kolesnichenko and E. V. Anslyn, *Chem. Soc. Rev.*, 2017, **46**, 2385–2390.
4 E. Mattia and S. Otto, *Nat. Nanotechnol.*, 2015, **10**, 111–119.
5 C. Schatz, S. Louguet, J. F. Le Meins and S. Lecommandoux, *Angew. Chem., Int. Ed.*, 2009, **48**, 2572–2575.
6 Y. Mai and A. Eisenberg, *Chem. Soc. Rev.*, 2012, **41**, 5969–5985.
7 D. E. Discher and A. Eisenberg, *Science*, 2002, **297**, 967–973.
8 A. Blanazs, J. Madsen, G. Battaglia, A. J. Ryan and S. P. Armes, *J. Am. Chem. Soc.*, 2011, **133**, 16581–16587.
9 S. Zhang, D. M. Marini, W. Hwang and S. Santoso, *Curr. Opin. Chem. Biol.*, 2002, **6**, 865–871.
10 S. Zhang, *Nat. Biotechnol.*, 2003, **21**, 1171–1178.
11 H. Yan, S. H. Park, G. Finkelstein, J. H. Reif and T. H. LaBean, *Science*, 2003, **301**, 1882–1884.
12 W. A. Petka, J. L. Harden, K. P. McGrath, D. Wirtz and D. A. Tirrell, *Science*, 1998, **281**, 389–392.
13 E. N. G. Marsh and W. F. DeGrado, *Proc. Natl. Acad. Sci. U. S. A.*, 2002, **99**, 5150–5154.
14 S. M. Douglas, H. Dietz, T. Liedl, B. Högberg, F. Graf and W. M. Shih, *Nature*, 2009, **459**, 414–418.
15 A. Aggeli, I. A. Nyrkova, M. Bell, R. Harding, L. Carrick, T. C. McLeish, A. N. Semenov and N. Boden, *Proc. Natl. Acad. Sci. U. S. A.*, 2001, **98**, 11857–11862.
16 C. Zhang, M. Su, Y. He, X. Zhao, P.-a. Fang, A. E. Ribbe, W. Jiang and C. Mao, *Proc. Natl. Acad. Sci. U. S. A.*, 2008, **105**, 10665–10669.
17 Y. He and C. Mao, *Chem. Commun.*, 2006, 968–969.

Published on 09 June 2017. Downloaded by East China University of Science & Technology on 10/23/2020 8:47:44 AM.

18 E. G. Bellomo, M. D. Wyrsta, L. Pakstis, D. J. Pochan and T. J. Deming, *Nat. Mater.*, 2004, **3**, 244–248.
19 K. L. Wooley, J. M. Fréchet and C. J. Hawker, *Polymer*, 1994, **35**, 4489–4495.
20 K. Okamoto and C. K. Luscombe, *Polym. Chem.*, 2011, **2**, 2424–2434.
21 D. Wu, Y. Huang, F. Xu, Y. Mai and D. Yan, *J. Polym. Sci., Part A: Polym. Chem.*, 2017, **55**, 1459–1477.
22 B. D. Olsen and R. A. Segalman, *Mater. Sci. Eng., R*, 2008, **62**, 37–66.
23 S. A. Jenekhe and X. L. Chen, *Science*, 1998, **279**, 1903–1907.
24 S. A. Jenekhe and X. L. Chen, *Science*, 1999, **283**, 372–375.
25 X. Wang, K. Cao, Y. Liu, B. Tsang and S. Liew, *J. Am. Chem. Soc.*, 2013, **135**, 3399–3402.
26 K. Cao, J. Ward, R. C. Amos, M. G. Jeong, K. T. Kim, M. Gauthier, D. Foucher and X. Wang, *Chem. Commun.*, 2014, **50**, 10062–10065.
27 J. Liu, Z. Guan, X. Tian, J. Lin and X. Wang, *Polym. Chem.*, 2016, **7**, 4419–4426.
28 K. Cao, N. Murshid, L. Li, A. Lopez, K. C. Tam and X. Wang, *Macromolecules*, 2015, **48**, 7968–7977.
29 T. Jiang, L. Wang, S. Lin, J. Lin and Y. Li, *Langmuir*, 2011, **27**, 6440–6448.
30 X. Zhu, Z. Guan, J. Lin and C. Cai, *Sci. Rep.*, 2016, **6**, 29796.
31 Y. Zhu, L. Fan, B. Yang and J. Du, *ACS Nano*, 2014, **8**, 5022–5031.
32 S. Arumugam, D. R. Vutukuri, S. Thayumanavan and V. Ramamurthy, *J. Am. Chem. Soc.*, 2005, **127**, 13200–13206.
33 Y. Zhu, L. Liu and J. Du, *Macromolecules*, 2012, **46**, 194–203.
34 X. He, M.-S. Hsiao, C. E. Boott, R. L. Harniman, A. Nazemi, X. Li, M. A. Winnik and I. Manners, *Nat. Mater.*, 2017, **16**, 481–488.
35 P. Khalatur, A. Khokhlov and D. Mologin, *J. Chem. Phys.*, 1998, **109**, 9614–9622.
36 C.-L. Fu, Z.-Y. Sun and L.-J. An, *J. Phys. Chem. B*, 2011, **115**, 11345–11351.
37 X. Li, M. Deng, Y. Liu and H. Liang, *J. Phys. Chem. B*, 2008, **112**, 14762–14765.
38 L. Guo and E. Luijten, *J. Polym. Sci., Part B: Polym. Phys.*, 2005, **43**, 959–969.
39 T. Azzam and A. Eisenberg, *Langmuir*, 2010, **26**, 10513–10523.
40 S. A. Meeuwissen, K. T. Kim, Y. Chen, D. J. Pochan and J. van Hest, *Angew. Chem., Int. Ed.*, 2011, **50**, 7070–7073.
41 K. T. Kim, J. Zhu, S. A. Meeuwissen, J. J. Cornelissen, D. J. Pochan, R. J. Nolte and J. C. van Hest, *J. Am. Chem. Soc.*, 2010, **132**, 12522–12524.
42 R. Rikken, H. Engelkamp, R. Nolte, J. Maan, J. van Hest, D. Wilson and P. Christianen, *Nat. Commun.*, 2016, **7**, 12606.
43 R. D. Groot and P. B. Warren, *J. Chem. Phys.*, 1997, **107**, 4423–4435.
44 M. E. Hogan and R. H. Austin, *Nature*, 1987, **329**, 263–266.
45 Y. Lu, B. Weers and N. C. Stellwagen, *Biopolymers*, 2001, **61**, 261–275.

 This journal is © The Royal Society of Chemistry 2017